

Controlled refraction and focusing of spin waves determined by the Aharonov-Casher effectV. N. Krivoruchko^{1,*} and A. S. Savchenko^{2,†}¹*Donetsk Physics & Technology Institute NAS of Ukraine, 46, Nauki Avenue, 03028 Kyiv, Ukraine*²*Peter Grünberg Institute and Institute for Advanced Simulation, Forschungszentrum Jülich
52425 Jülich, Germany*

(Received 28 February 2024; revised 8 May 2024; accepted 8 May 2024; published 22 May 2024)

The influence of an external static electric field on spin wave (SW) dynamics leads to an additional topological phase called the Aharonov-Casher (AC) phase. It is manifested as a shift in dispersion and the group velocity direction of the spin wave under the electric field. Within a linear approximation, the AC effect can be considered by including the Dzyaloshinskii-Moriya-like interaction between neighboring spins, which is proportional to the applied electric field. In this paper, we use these findings to examine the possibility of the electric field control of the refraction of coherently propagating SWs. This is done by studying the propagation SWs across the boundary between two regions of a homogeneous ferromagnetic film under the influence of different external electric fields. We have derived an analytical expression for a magnetic Snell's law and performed micromagnetic simulations to demonstrate how the AC phase shift can control SW refraction. This effect enables us to quantify the topological AC phase action. It presents a promising approach for guiding and manipulating the phase and energy flow of SWs using an external electric field, opening a way to control magnonic devices.

DOI: [10.1103/PhysRevB.109.184437](https://doi.org/10.1103/PhysRevB.109.184437)**I. INTRODUCTION**

The fundamental characteristics of spin waves (SWs) are phase, amplitude, and propagation direction. Among the important challenges motivating research activities in magnonics [1–4] is finding mechanisms to operate these SW properties. In optics, one of the spatially efficient methods to control waves is reflection and refraction at an interface between two materials with different optical parameters. Although a magnetic field can influence magnetic characteristics, these types of SW operations usually have significant spatial coverage. It makes the compatibility of magnonic devices with conventional voltage-controlled semiconductor electronics more difficult. The possibility of using, e.g., an electric voltage to manipulate the magnetic parameters of a system and thus the dispersion relation of SWs has been intensively discussed in recent reports [5–12] driven by its physics and enormous potential for applications in magnonic devices (see review articles [13–15] for details).

An external electric (\mathbf{E}) field is also investigated as one of the alternative and efficient solutions to control the SW dispersion and, thus, the phase and power flow of SWs. Indeed, it has been shown [16–20] that an external static electric field causes a frequency shift of SWs, like the Dzyaloshinskii-

Moria (DM) interaction, even in a ferromagnet where the inversion symmetry is presented. It is a typical case of a quantum topological effect in solid-state physics. According to the quantum mechanics paradigm, the voltage control of the magnetic parameters implies a modification of local (Landau) system parameters. The influence of the electric field on SW energy is an example of a global—*topological*—effect in the magnetization dynamics [21–26]. In particular, the orbital motion of neutral magnetic moments in a static electric field produces an extra—a topological origin—phase, the so-called Aharonov-Casher (AC) phase [21,22]. In the first approximation, the influence of this field on magnetization dynamics is equivalent to the generation of a DM-like interaction between the neighboring spins \mathbf{S}_i and \mathbf{S}_j . Thus, the effect can be considered by being written in a conventional form as $\mathbf{d}_{ij} \cdot (\mathbf{S}_i \times \mathbf{S}_j)$. Here, the vector \mathbf{d}_{ij} is orthogonal to the unit vector \mathbf{e}_{ij} along the line connecting the neighboring spins and the electric field \mathbf{E} [16–19]. The calculations [17–19] based on the superexchange model give $\mathbf{d}_{ij} = \xi_{SO} J e (\mathbf{E} \times \mathbf{e}_{ij})$, where e is the elementary charge value, J stands for the Heisenberg exchange coupling, and ξ_{SO} is the spin-orbit coupling. Zhang *et al.* [20] showed, using experimental data on YIG (yttrium iron garnet, $\text{Y}_3\text{Fe}_5\text{O}_{12}$), that the SW's phase control by an external electric field could be effectively implemented in thin ferromagnet films. Recently, Serga *et al.* [27] proved in their experimental research that magnons could accumulate an additional phase when interacting with an electric field through the AC effect. They used two types of magnetostatic SW propagating perpendicularly and parallel to the film magnetization direction in YIG, which revealed the AC effect contribution in the SW phase change.

The theoretical analysis confirms that the AC phase induced by an external electric field could effectively control the

*krivoruc@gmail.com

†a.savchenko@fz-juelich.de

SW power flux and caustics in thin ferromagnet films [28]. The conjunction of the magnetodipole interaction and SWs coupling to the electric field also reveals itself in nonreciprocal unidirectional caustic beams of dipole-exchange coupled SWs [29]. An important practical consequence is that changing the sign of the electric field changes the shifts of the SW's group velocity, allowing for the SW focusing condition to be obtained.

It has been also demonstrated that heterochiral magnetic structures with DM interaction are an ideal platform for adaptable waveguides for SW [30–35]. In particular, Yu *et al.* showed that the scattering of SWs at a domain wall in a single magnetic material with DM interaction can be described using the generalized Snell's law [30]. In Ref. [32], the propagation and reflection of SWs at interfaces of magnetic films with different DM strengths were examined. It was found that SWs may experience a total reflection at interfaces of regions with different DM strengths, similar to total optical reflection at interfaces. Wang *et al.* analyzed the dynamics of SW in a nonuniform electric field from the point of view of the mechanism of generation and control of the magnon spin current by an external electric field [36]. The presented analytical and numerical results show that this mechanism of spin current generation can become a competitive alternative to the thermal one.

In this paper, we investigate the effect of the DM-like interaction induced by a static external electric field on the propagation of exchange and dipole-exchange SWs in a thin ferromagnetic film. The findings of Refs. [16–20,28,29,37] are employed to examine how an electric field can control the refraction of SWs as they cross a boundary between regions where different DM-like interactions are present due to \mathbf{E} fields of a different magnitude. We will first obtain analytical expressions for the reflection and transmission of SWs at such an interface. It has been demonstrated that the scattering of SWs at such a boundary follows a generalized Snell's law in analogy to an optical fiber [31,32,34,35]. Due to the DM-like effect (the AC phase) caused by an applied electric field, these two regions act as magnetic media with different propagation dynamics of SWs. Based on these findings, we have conducted micromagnetic simulations to investigate the effectiveness of the electric field in controlling the refraction of coherently propagating SWs. We demonstrate how these peculiar phenomena can be used as an alternative method (used in Ref. [20]) to quantify the topological phase magnitude. Moreover, this makes it possible to distinguish between the Aharonov-Casher effect and the contributions of magnetoelectric effects simply by measuring the angles of incident and refracted SW beams. Our results point to an important avenue for manipulating SWs and developing electrically tunable magnonic devices. Some preliminary results of this study can be found in Ref. [38].

The paper is structured as follows: In the next section (Sec. II), we briefly describe the model under consideration. In Sec. III, the analytical expression of magnetic Snell's law is presented for the scattering of SWs at the interface between two parts of a magnetic film under different external electric fields. To establish the exclusive effect of the \mathbf{E} field, we performed the analytical calculations for the exchange SWs when the demagnetizing fields can be neglected. The

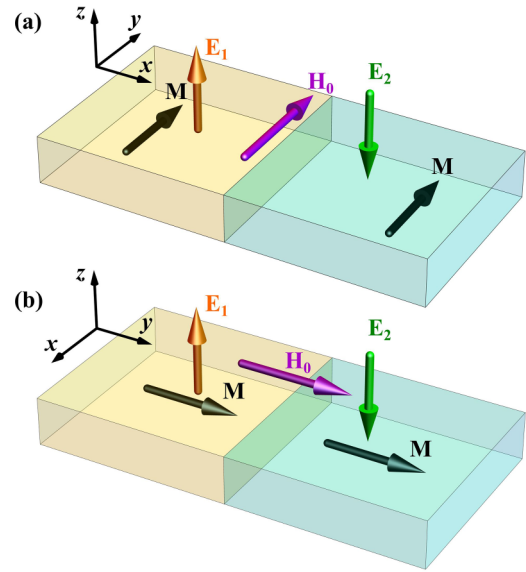


FIG. 1. Schematic illustration of the in-plane magnetized film. The electric field is normal to the film. Please note the rotation of the coordinate system (a) and (b).

analytical results for the refraction of the SWs are confirmed by micromagnetic simulations presented in Secs. IV and V. Here, a more rigorous expression for the SW dispersion is used (the details are given in the Appendix and Supplemental Material). The simulations are performed for the classical magnetic material $\text{Y}_3\text{Fe}_5\text{O}_{12}$, and they suggest that controlling Snell's law for SWs using an electric field may be experimentally feasible. Section VI summarizes the main conclusions.

II. THE MODEL

Let us consider exchange SWs propagating in a homogeneous ferromagnetic film with the magnetization vector \mathbf{M} aligned in the $x - y$ plane of the film, and the external magnetic field \mathbf{H}_0 is applied along the $+y$ direction. The left/right side of the film is under the effect of static external electric fields $\mathbf{E}_{1(2)}$ along the $\pm z$ direction, see Fig. 1. Our focus will be on the reflection and transmission of SWs through an “interface”—the boundary between the film regions under the action of electric fields \mathbf{E}_1 and \mathbf{E}_2 . To identify the effect of the \mathbf{E} -field-induced DM-like interaction exclusively, we discuss in our analytical study (Secs. II and III) the simplest case where a uniaxial anisotropy field \mathbf{H}_A is strong enough and the demagnetizing field can be neglected. However, our numerical simulations consider the dynamical dipolar fields originating from the magnetization precession (Secs. IV and V). We focus solely on the effect of \mathbf{E} -field-induced DM-like interaction. To achieve this, we make two assumptions: (i) other magnetic parameters are homogeneous throughout the film, and (ii) we assume that the SW wave vector \mathbf{k} and the \mathbf{E} field are mutually orthogonal, the \mathbf{E} field is normal to the film plane, and the Doppler shift vanishes. The Doppler shift disappears when the electric field and wave vector of the SW are perpendicular to each other, see, e.g., Ref. [39]. Note that the SW's Doppler shift plays a dominant role in the magnetization dynamics of rare-earth metals, and it is proportional to the mobility of the

spin-polarized electrons. However, in the case of localized spins in a magnetic dielectric, this effect is several orders of magnitude smaller than the similar effect in the collective magnetization dynamics of spin-polarized electrons (the band theory of magnetism in metals). If the localized spins are coupled by unpolarized electrons (the Ruderman-Kittel-Yosida model), the SWs' Doppler shift will be second-order relative to the spin-polarized electrons [40]. More details of the uniform current effects on SWs in ferromagnetic metals can be found in Refs. [40,41]. Assuming that the SWs' Doppler shift is negligible, we discuss two geometries below: the magnetization \mathbf{M} of the film is parallel [Fig. 1(a)] and perpendicular [Fig. 1(b)] to the film boundary introduced by the \mathbf{E} field.

The magnetization dynamics is described by the Landau-Lifshitz equation

$$\frac{\partial \mathbf{M}}{\partial t} = -\gamma \mu_0 \mathbf{M} \times \mathbf{H}_{\text{eff}}.$$

Here γ stands for the gyromagnetic ratio, μ_0 is the vacuum permeability, the magnetization $\mathbf{M} = \mathbf{M}(\mathbf{r}, t) = \mathbf{M}_S + \mathbf{m}(\mathbf{r}, t)$, where \mathbf{M}_S stands for the uniform equilibrium magnetization of constant amplitude and $\mathbf{m}(\mathbf{r}, t)$ is the deviation from equilibrium. The total effective magnetic field \mathbf{H}_{eff} comprises contributions from the exchange field $\mathbf{H}_{\text{ex}} = J \nabla^2 \mathbf{M}(\mathbf{r})$ (J is the exchange coupling), the magnetic uniaxial anisotropy field $\mathbf{H}_A \parallel y$, and the electric field induced DM-like interaction of the form [18,19] $\mathbf{H}_E = 2\mathbf{d}_E \times (\mathbf{e}_{ij} \cdot \nabla)\mathbf{m}$. As noted above, the vector \mathbf{d}_E is given by $\mathbf{d}_E = \xi_{SO} J (e\mathbf{E} \times \mathbf{e}_{ij})$; here, the unit vector \mathbf{e}_{ij} is along the line that connects the magnetic moments between points i and j ; e is the elementary charge value, and ξ_{SO} is proportional to the spin-orbit interaction strength. In this subsection, the dipolar interaction and the damping term are neglected to illustrate the electric field effect.

The SW propagation and dispersion relation in ferromagnetic films has been studied earlier in detail [42]. In this section, we will focus on the exchange SWs of high frequencies and the SW dispersion relations in ferromagnetic media affected by the static electric field $\mathbf{E}_{1(2)} = E_{1(2)}\mathbf{e}_z$. Following Refs. [30,31,33,34], we can present the dispersion relation as

$$\frac{\omega_{1(2)}(\mathbf{k})}{\gamma \mu_0} = H_0 + H_A + Dk^2 - M_S \lambda_{SO} E_{1(2)} k_x, \quad (1)$$

where $\omega(\mathbf{k})$ is the angular frequency of the wave, $|\mathbf{M}_S| = M_S$ is the magnetization saturation, $D = JM_S$, the wave vector \mathbf{k} is in the film's plane $k = (k_x^2 + k_y^2)^{1/2}$, $\lambda_{SO} = 2J\xi_{SO}|e|$, and H_A stands for the magnetic uniaxial anisotropy. The last term in Eq. (1) describes the electric field effect on SW dynamic. It causes the isofrequency ellipses to move in the direction of $(\mathbf{E} \times \mathbf{M}_S)$. In Fig. 1(a) geometry, the shift is *perpendicular* to the boundary that separates the regions of the film affected by different electric fields. In Fig. 1(b) geometry, the isofrequency ellipses are shifted *parallel* to the \mathbf{E} -field boundary regions. This shift is equal to $M_S \lambda_{SO} E_{1(2)}$ for both cases. Figure 2 illustrates how the isofrequency contours of the *exchange* SWs shift under the effect of the applied electric field at different frequencies for the geometries in Fig. 1.

We would like to highlight two significant differences between our study and previous studies regarding the scattering behavior of SWs in chiral magnetic films with DM interaction [30,31]. In these cases [30,31], the isofrequency ellipses of the SWs are pushed *parallel* to the domain's boundary

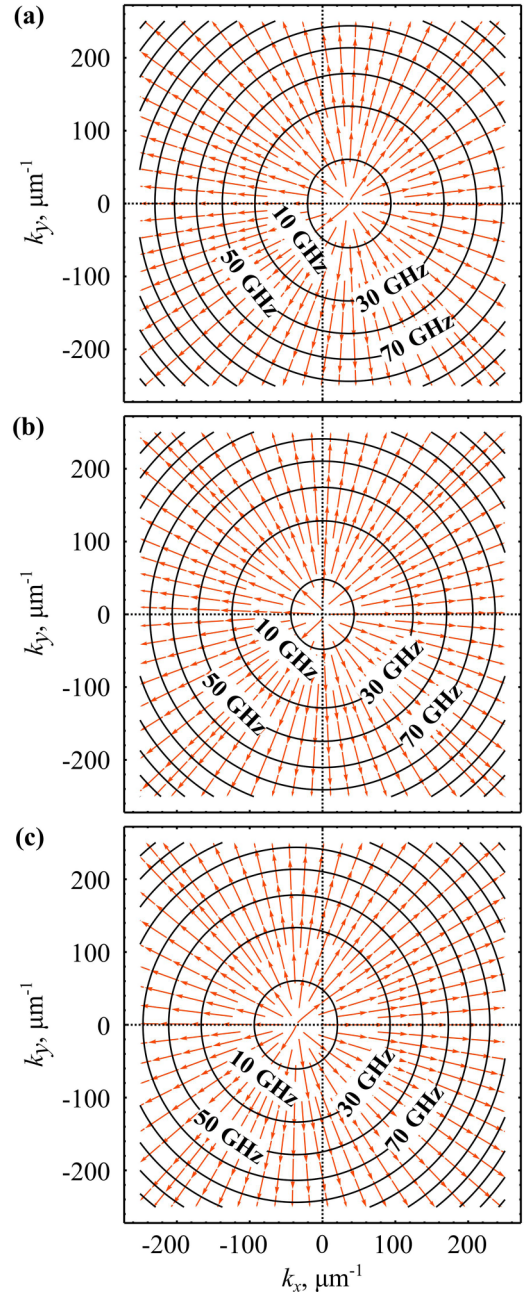


FIG. 2. The isofrequency contours shift of exchange SWs [the black curves, Eq. (1)] under the effect of the applied electric field at different frequencies for the geometry in Fig. 1: (a) $E = 0.7$ V/nm, (b) $E = 0$ V/nm, (c) $E = -0.7$ V/nm. The group velocity (red lines with arrows) was obtained from Eq. (2). The material parameters used for YIG are in the Appendix.

due to a conventional DM interaction. In our case, due to the electrically induced DM-like interaction, the isofrequency circles can be shifted by the \mathbf{E} field normal or parallel to the actual boundary regions of the film. This depends on whether the magnetization \mathbf{M} of the film is parallel or perpendicular to the boundary.

The shift of the isofrequency circles in the up/down electric field domains, Eq. (1), has significant consequences for the reflection and refraction of an incoming SW at the boundary between magnetic film regions with different DM-like

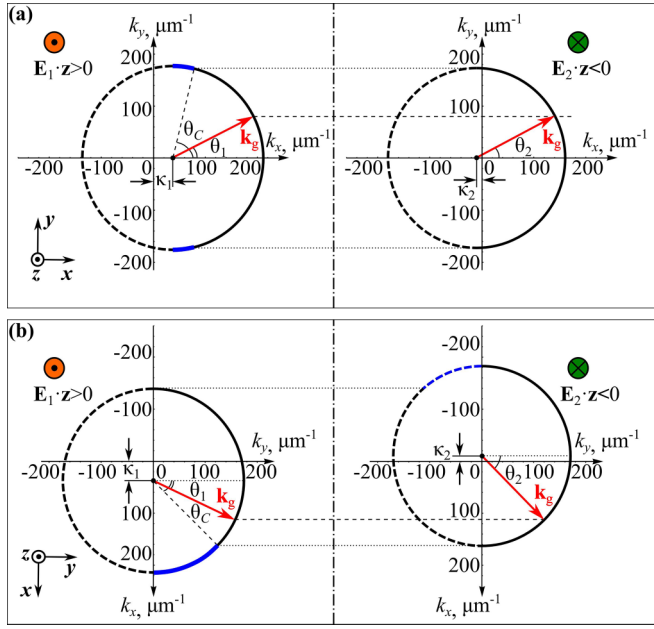


FIG. 3. Refraction of an incoming SW at the interface between regions of the magnetic film subject to different external electric fields. (a) Magnetization is parallel to the \mathbf{E} -field boundary (dash-dotted line); (b) magnetization is perpendicular to the \mathbf{E} -field boundary. The blue color corresponds to the area of incident angles where SW is completely reflected. Numerical estimation was performed for YIG films with a thickness of 10 nm, $E_1 = 0.7$ V/nm, and $E_2 = -0.2$ V/nm.

interactions (regions with different AC phases). In the following sections, we derive an analytical expression for a generalized magnetic Snell's law and examine how, by using a moderate external electric field, one can control SW refraction and reflection at interfaces between regions with different AC phase shifts. For the reader's convenience, we take advantage of geometric interpolation and the fact that exchange spin waves can be described by circular isofrequency contours [30–33].

III. MAGNETIC SNELL'S LAW FOR SPIN WAVES

Magnetization is parallel to the E-field boundary. Let us begin the discussion with the geometry where the \mathbf{E} -field boundary is parallel to the magnetization and the isofrequency ellipse is shifted along the normal to this boundary, as shown in Fig. 1(a). When the SW with an angle of incidence θ_1 (the angle of the group velocity to the interface normal $+\mathbf{e}_x$ direction) is incident from the left side of the film to the right side, it is refracted with an outgoing angle θ_2 , see Fig. 3(a). The SW keeps the angular frequency after reflection $\omega_r(\mathbf{k}_r)$ and transmission $\omega_t(\mathbf{k}_t)$, i.e., $\omega(\mathbf{k}) = \omega_r(\mathbf{k}_r) = \omega_t(\mathbf{k}_t)$ where \mathbf{k} , \mathbf{k}_r , and \mathbf{k}_t are wave vectors incident, reflected and transmitted SWs correspondingly. The continuity of the wave vector along

the interface is guaranteed by translational symmetry, so the SW fronts must coincide at the \mathbf{E} -field boundary. The SW's group velocity is

$$\begin{aligned} \mathbf{v}_{g1(2)} &= \partial\omega_{1(2)}(\mathbf{k})/\partial\mathbf{k} = \gamma\mu_0(2D\mathbf{k} - M_S\lambda_{SO}E_{1(2)}\mathbf{e}_x) \\ &= 2\gamma\mu_0D\mathbf{k}_{g1(2)}. \end{aligned} \quad (2)$$

Here we introduce the radius of the isofrequency circle $|\mathbf{k}_{gi}| = k_{gi}(\omega) = \{(\omega/\gamma\mu_0 - H_A - H_0)/D + \kappa_i^2(E_i)\}^{1/2}$, where $\kappa_i(E_i) = M_S\lambda_{SO}E_i/2D$ is the magnitude of the isofrequency circle displacement. Thus, to fulfill the first part of the wave vector continuity relations, the conservation of $\mathbf{k}||\mathbf{y}$: $k_{gy} = k_{gry}$, the reflection angle must be equal to the incident angle. Referring to Eq. (2), the second part of the relations, $k_{gry} = k_{gty}$, leads to the Snell-like law in geometrical optics for SWs. The generalized (magnetic) Snell's law, $k_{g1}(\omega) \sin\theta_1 = k_{g2}(\omega) \sin\theta_2$, is now equal to

$$\begin{aligned} &\{(\omega/\gamma\mu_0 - H_A - H_0)/D + \kappa_1^2(E_1)\}^{1/2} \sin\theta_1 \\ &= \{(\omega/\gamma\mu_0 - H_A - H_0)/D + \kappa_2^2(E_2)\}^{1/2} \sin\theta_2. \end{aligned} \quad (3)$$

The SW's incidence/refraction angles relation, Eq. (3), is derived for the interface formed in a homogeneous magnetic film subjected to different external electric fields. It differs from Snell's laws, obtained for interfaces created by two magnetic domains [30] or between two regions with different magnetic properties [43–47]. It is like a generalized Snell's law in Ref. [32] for a magnetic structure with DM interaction in opposite directions. In our case, as in the case considered by Mulkers *et al.* [32], the isofrequency ellipse shifts in the left and right areas of \mathbf{k} space are not symmetric: $\kappa_1(E_1) \neq \kappa_2(E_2)$, as shown in Fig. 3(a). In addition, in our case, the magnitude of the isofrequency ellipse shift in \mathbf{k} space can be controlled simply by tuning the strength of an external static electric field.

In Eq. (3), we have two free parameters, $E_{1(2)}$, and thus, the SW reflection can be tuned by adjusting the applied electric field strength. According to Eq. (3), total reflection, $\theta_2 = \pi/2$, occurs when $\kappa_2^2(E_2) < \kappa_1^2(E_1)$ and the incident angle θ_1 satisfies the condition $\theta_C < |\theta_1| < \pi/2$ [see Fig. 3(a)] with the critical angle

$$\sin\theta_C = \left\{ \frac{(\omega/\gamma\mu_0 - H_A - H_0)/D + \kappa_2^2(E_2)}{(\omega/\gamma\mu_0 - H_A - H_0)/D + \kappa_1^2(E_1)} \right\}^{1/2}. \quad (4)$$

When $|E_1| \leq |E_2|$, all the incident SWs are refracted. So, the SW propagation and reflection conditions are controllable by the E_2/E_1 ratio.

Magnetization is perpendicular to the E-field boundary. If the magnetization is normal to the \mathbf{E} -field boundary, Fig. 1(b), the isofrequency ellipses are shifted along this boundary. In Fig. 1(b), the angle of incidence θ_1 is now the angle of the group velocity to the interface normal $+\mathbf{e}_y$. Snell's magnetic law and the equation for θ_C for this geometry have the following forms:

$$\{(\omega/\gamma\mu_0 - H_A - H_0)/D + \kappa_1^2(E_1)\}^{1/2} \sin\theta_1 + \kappa_1(E_1) = \{(\omega/\gamma\mu_0 - H_A - H_0)/D + \kappa_2^2(E_2)\}^{1/2} \sin\theta_2 - \kappa_2(E_2), \quad (5)$$

$$\sin\theta_C = \frac{\{(\omega/\gamma\mu_0 - H_A - H_0)/D + \kappa_2^2(E_2)\}^{1/2} - [\kappa_1(E_1) + \kappa_2(E_2)]}{\{(\omega/\gamma\mu_0 - H_A - H_0)/D + \kappa_1^2(E_1)\}^{1/2}}. \quad (6)$$

In this case, the incidence angle intervals for refraction and total reflection are asymmetric with respect to the sign of θ_1 [see Fig. 3(b)], except when $\kappa_1(E_1) = -\kappa_2(E_2)$. The critical angle can take any value between $-\pi/2$ and $\pi/2$, depending on the $\kappa_i(E_i)$, and the applied electric field. In the absence of an electric field ($E_{1,2} = 0$), the angle $\theta_C = \pi/2$ and all incident SWs are propagated. The unconventional refraction and reflection of SW are caused by the extra topological phase, called the AC phase [21,22], induced by the \mathbf{E} field. Like the case of a conventional DM interaction [48], SWs in a system with \mathbf{E} -field-induced DM-like interaction have an anisotropic dispersion relation. The anisotropy of energy dispersion can cause a noncollinearity between the wave vector \mathbf{k} and the group velocity \mathbf{v}_g , see Eq. (2). The phase velocity of SWs also depends on the angle between the magnetization \mathbf{M} and the wave vector \mathbf{k} . As a result, the boundary between regions with different electric fields acts as an abrupt magnetic boundary for SWs.

As noted in the Introduction, it was recently found that SW total reflections and negative refractions could occur at the interface due to DM interactions [31,32]. SW refractions can be nonsymmetric at positive and negative incidence angles in those cases. Additionally, it was shown that the magnonic Goos-Hänchen (GH) effect of SW beams occurs when SWs are totally reflected at the interface and vanish otherwise [35,49]. The GH effect for SWs is a promising way to study magnetic interface properties [33,49–53] and manipulate the SW phase. The electric field controlling the GH shift will be discussed elsewhere. This paper focuses on demonstrating the effectiveness of \mathbf{E} -field control on SW refraction. To verify our analytical results, we examine the external electric field controllability of the refraction of coherently propagating SWs using numerical verifications and micromagnetic simulations. These simulations have been performed in MuMax3 [54] using the parameters previously estimated for YIG films [55,56] (see the details in Appendix).

IV. DISPERSION RELATION, REFRACTION OF EXCHANGE SPIN-WAVE

This section examines the refraction processes at the \mathbf{E} -field boundary for exchange SW. We perform an analysis using the expression for the SW dispersion that considers dynamic dipolar fields originating from the magnetization precession (see, e.g., Refs. [19,40]). Within the standard approach [40], the dispersion relation for the SW spectrum in the film with $\mathbf{H}_0 \parallel \mathbf{M}_S \parallel \mathbf{y}$, $\mathbf{k} \in xy$ (Fig. 1) can be expressed as

$$\omega(E, k) = \gamma \mu_0 [H_x(k) H_y(k)]^{1/2} - \omega_E(k). \quad (7)$$

Here

$$H_x(k) = H_0 + Dk^2 + M_S g(kd) \sin^2 \varphi_k, \quad (8)$$

$$H_y(k) = H_0 + Dk^2 - H_K + M_S [1 - g(kd)], \quad (9)$$

$$\omega_E(k) = \gamma \mu_0 M_S \lambda_{SO} E k_x = \omega_M \lambda_{SO} E k_x, \quad (10)$$

with wave vector $k = (k_x^2 + k_y^2)^{1/2}$, d is the film thickness, $g(kd) = \{1 - [1 - \exp(-kd)]/kd\}$, $\varphi_k = \arctan(k_x/k_y)$, $H_K = 2K_u/\mu_0 M_S$ stands for the effective anisotropy field, and K_u is the magnetic anisotropy. From Eqs. (7)–(10) one finds

that not only the external electric field but also the dipolar coupling $g(kd)$ contributes to linear in k dependence of the SW spectrum $\omega(k)$. However, there is an essential distinction between these two constituents. The contribution due to the electric field, Eq. (10), is anisotropic, k_x , and its sign depends on both the wave vector \mathbf{k} and the magnetization directions. In contrast, the dipolar (magnetostatic) component does not. Thus, in addition to an ellipticity in the precession, the external electric field “manifests” itself in a nonreciprocity of the SW propagation $\omega(\mathbf{k}) \neq \omega(-\mathbf{k})$. These features make it possible to unambiguously distinguish the \mathbf{E} -field effect from the dipolar coupling contribution in an experiment.

Our analysis will use isofrequency curves derived from Eqs. (7)–(10). We begin with the case where the exchange term dominates the SW dynamics. So, we will consider exchange SWs to which large \mathbf{k} vectors correspond.

Exchange spin waves. As mentioned above, the exchange SWs have a more isotropic dispersion relation than the dipole-exchange excitations [42]. Their isofrequency curves are near-circular [30–33], which is also apparent in their refraction. In this case, Snell’s law [(3) and (5)] can be obtained in the exchange limit from Eqs. (7)–(10), considering the continuity of the wave vector component directed along the \mathbf{E} -field boundary.

In our numerical verifications for exchange SWs, we suggested that the normal constant electric field $E_z = \pm 0.7$ V/nm (see Fig. 1) influences one half of the film and $E_z = 0$ on the other half. The YIG film has a thickness of $d = 10$ nm. Other material parameters and details of simulations are in the Appendix. Figures 4 and 5 illustrate the micromagnetic simulation of refraction at the \mathbf{E} -field boundary and isofrequency curves obtained from Eqs. (7)–(10) for the exchange SW. In these figures, \mathbf{k}_i is the wave vector of an incident SW, \mathbf{k}_r represents the wave vector of the refracted SW, and \mathbf{v}_g is the group velocity direction of the SWs ($\mathbf{v}_g \parallel \mathbf{k}_g$). In the simulated snapshots (Figs. 4 and 5), the spin wave was excited by the *rf* field applied locally (antenna) in a region located on the $\mathbf{E} = 0$ side of the film. The details of excitation are described in the Appendix. The red and blue colors represent the dynamic deviation from the equilibrium magnetization distribution for the SW propagating in each half-space; red arrows indicate the group velocities of SW; the phase velocities are parallel to \mathbf{k} and directed along the normal to the wave fronts.

In the geometry depicted in Fig. 4, \mathbf{M}_S is parallel to the \mathbf{E} -field boundary, and the SWs with all the incidence angles refract to the area with $E_z = \pm 0.7$ V/nm, according to Eqs. (3) and (4). In this case, the \mathbf{E} -field influence leads to the changing wavelength of the refracted SW. The increasing or decreasing of this wavelength depends on the positive [Fig. 4(a)] or negative [Fig. 4(b)] sign of E_z , respectively.

When the \mathbf{M}_S is perpendicular to the \mathbf{E} -field boundary, it is possible to manipulate the refraction condition of the spin wave by the electric field. It is illustrated in Fig. 5. Here, the sections of the isofrequency curves marked in blue correspond to the total internal reflection. The condition of its realization can be derived from Eqs. (5) and (6). When half of the film is under the field $E_z > 0$, negative refraction takes place at $0 < k_x < M_S \lambda_{SO} E_z / 2D$ [it is marked as the orange region in Fig. 5(a)]. This effect is characterized by the

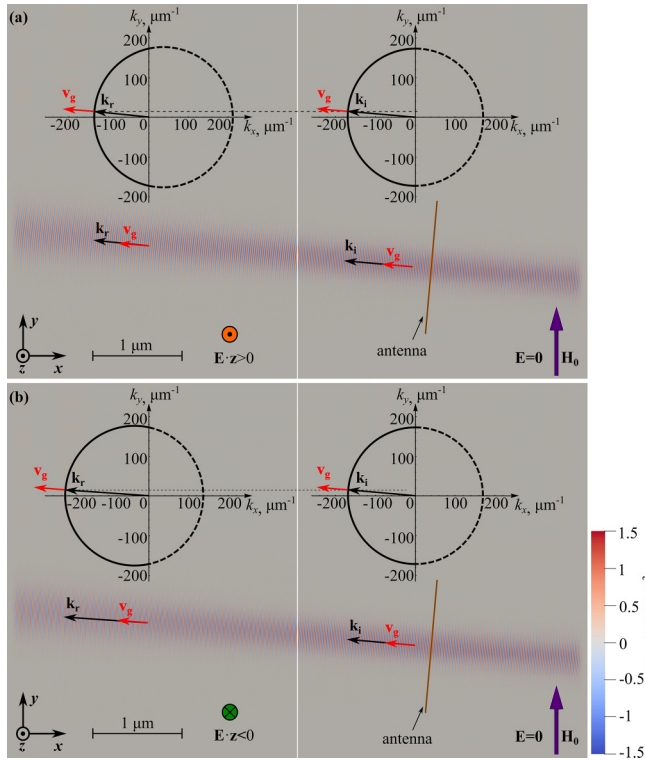


FIG. 4. Exchange SW refraction on the boundary of the magnetic film consisting of two half-spaces with $E_z \neq 0$ and $E_z = 0$. $\mathbf{H}_0 \parallel \mathbf{M}_S$ [see Fig. 1(a)]; $|E_z| = 0.7$ V/nm and $E_z = 0$; $f = 50.0$ GHz. Under the effect of the \mathbf{E} field, the isofrequency ellipse is shifted *normally* to this boundary. (a) $E_z > 0$; (b) $E_z < 0$.

projections of group velocities: the \mathbf{v}_g of incident and \mathbf{v}_g of refracted waves have opposite signs on the \mathbf{E} -field boundary. The micromagnetic simulation results in Fig. 5(a) illustrate

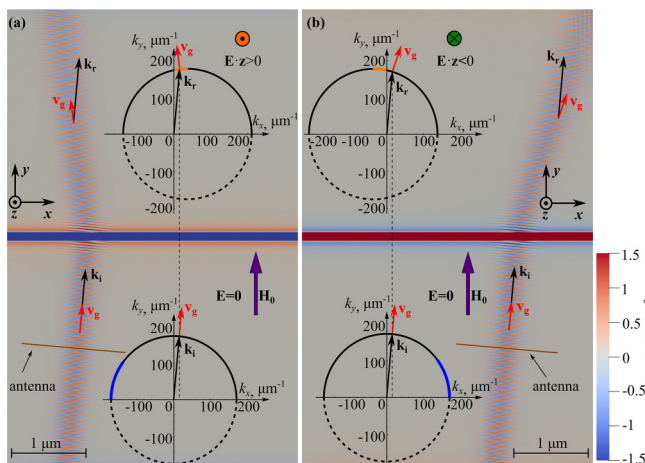


FIG. 5. Same as Fig. 4 but for $\mathbf{H}_0 \parallel \mathbf{M}_S$ normal to the boundary [Fig. 1(b)] and a subsequent shift of the isofrequency ellipse *along* the boundary. The blue lines on isofrequency curves correspond to the areas of incident angles where SW is completely reflected. The orange lines are the regions with a negative refraction effect. The region of magnetization twisting near the \mathbf{E} -field boundary is marked by red and blue colors.

this case of refraction. It should be noted that the magnetization twist near the \mathbf{E} -field boundary in Fig. 5 is marked in red and blue. This twist can be explained by analogy with [57,58] due to the appearance of magnetic boundary conditions at the \mathbf{E} -field boundary as a result of different induced DM-like interactions.

For $E_z < 0$ [Fig. 5(b)], negative refraction exists at $M_S \lambda_{SO} E_z / 2D < k_x < 0$, while normal SWs refraction occurs for other k_x values, corresponding to the black sections of isofrequency curves in Fig. 5. Similar asymmetric refraction of SWs can also be realized in thin ferromagnetic films at the interface with different DM interactions [31,32,35]. However, in the considered case of the induced DM-like interaction, the refraction mode can be manipulated by using the \mathbf{E} field.

The analysis of isofrequency curves and micromagnetic simulations show excellent agreement in the refraction results in Figs. 4 and 5. In particular, this applies to the directions and values of the wave vector of the incident and refracted SWs at a given frequency. Additionally, the results of the micromagnetic refraction simulations are demonstrated in the Supplementary Material [59] in the movies 4a.mp4, 4b.mp4, 5a.mp4, and 5b.mp4, which correspond to the cases presented in Figs. 4(a), 4(b) 5(a), and 5(b).

In order to realize the electric-field-induced features of SW refraction in the dipolar-exchange regime, a lower \mathbf{E} -field strength is required compared to exchange SWs. Unlike exchange SWs, for dipole-exchange SWs, only expressions (7)–(10) remain valid, and the isofrequency curves are not circular.

V. REFRACTION AND FOCUSING OF DIPOLE-EXCHANGE SPIN WAVE

For the dipolar-exchange regime, we assumed that the electric field, applied to the half of the YIG film, is $E_z = \pm 0.35$ V/nm, the SW frequency $f = 7.9$ GHz, the external magnetic field $\mu_0 H_0 = 0.2$ T, and the film thickness is 30 nm (see Appendix for details). The isofrequency curves obtained from (7)–(10) illustrate the effect of static electric field on the refraction of dipole-exchange SWs in Fig. 6.

Magnetization is parallel to the E-field boundary. Let us consider a scenario where the magnetization \mathbf{M}_S is directed along the interface between the electric fields' areas [as shown in Fig. 1(a)]. The volume dipolar-exchange SW falls from the right part of the film with $E_z = 0$ to the left area with $E_z \neq 0$ (Fig. 6). Let us consider the isofrequency curves in Fig. 6. The interval of wave numbers $-33.6 \mu\text{m}^{-1} < k_y < 33.6 \mu\text{m}^{-1}$ covers all incidence angle values. The points of intersection of the isofrequency curves with the k_y axis on the right part of the film ($E_z = 0$) in Fig. 6 indicate this. When the \mathbf{E} field is along the z axis ($E_z = \pm 0.35$ V/nm) in the left area of the YIG film, the isofrequency curve has the form shown in Fig. 6. There is no region of total internal reflection because the wave number intervals k_y of the isofrequency curve at $E_z = 0$ are narrower than for the case $E_z \neq 0$. The SW refraction is different for positive and negative \mathbf{E} -field directions. It occurs because the isofrequency curves are deformed and shifted oppositely in \mathbf{k} space in the \mathbf{E} -field-affected regions. At $E_z > 0$ [Fig. 6(a)], positive refraction is observed outside

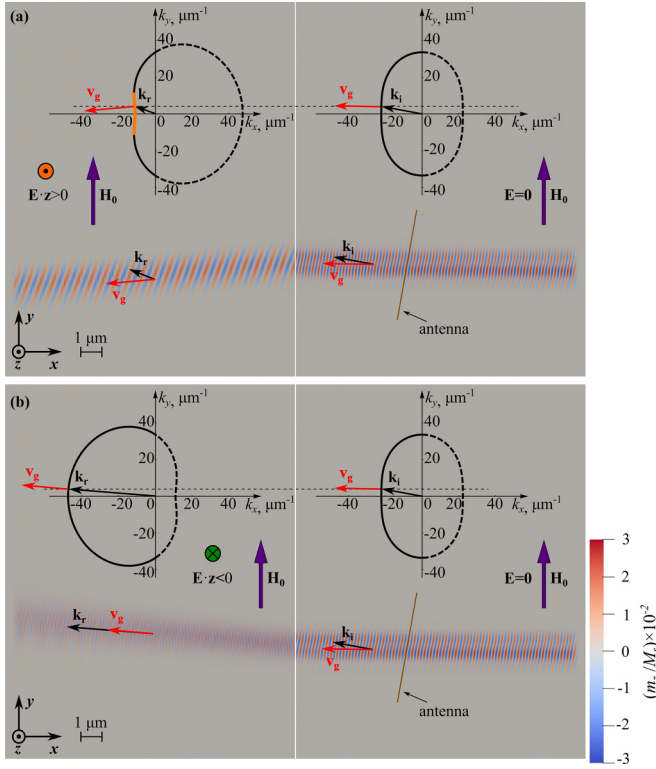


FIG. 6. The dipole-exchange SW refraction on the boundary of the magnetic film consisting of two half-spaces, with $E_z \neq 0$ and $E_z = 0$. $\mathbf{H}_0 \parallel \mathbf{M}_S$ parallels to the boundary between areas with $|E_z| = 0.35$ V/nm and $E_z = 0$. Under the effect of the \mathbf{E} -field, the isofrequency curve moves *normally* to this boundary. The SW frequency $f = 7.9$ GHz. The orange line is the region with a negative refraction effect. (a) $E_z > 0$; (b) $E_z < 0$.

of the interval $-11.4 \mu\text{m}^{-1} < k_y < 11.4 \mu\text{m}^{-1}$. However, inside the interval $-11.4 \mu\text{m}^{-1} < k_y < 11.4 \mu\text{m}^{-1}$, the group velocity of the refracted and incident waves has the opposite sign projections on the $E_z(=0)/E_z(\neq 0)$ interface, and a negative refraction effect will take place. Suppose the direction of the \mathbf{E} field switches to the opposite [Fig. 6(b)]. In this case, the isofrequency curve has a positive curvature at $k_x < 0$, and the spin wave will have positive refraction at all incidence angles. Thus, when the \mathbf{M}_S vector is directed along the interface between regions with $E_z = 0$ and $E_z \neq 0$, the switching from positive to negative refraction can be executed by reversing the \mathbf{E} -field sign. The results of the micromagnetic simulations in Fig. 6 perfectly agree with the refraction processes illustrated on the isofrequency curves, which are obtained from the analysis of analytical expressions (7)–(10).

Note that in the interval $-11.4 \mu\text{m}^{-1} < k_y < 11.4 \mu\text{m}^{-1}$, the isofrequency curve at $E_z > 0$ contains a section symmetric about the k_y axis and has negative Gauss curvature. This section is marked in orange in Fig. 6(a). Since \mathbf{v}_g is directed along the normal to the isofrequency curve, the focusing of the spin waves can be realized for the abovementioned interval of k_y . It is similar to the case in Ref. [60], where the focusing features of SWs induced by the dipole-dipole interaction in synthetic antiferromagnets have been studied.

Figure 7 shows an example of SW focusing controlled by the constant electric field. In this case, we use two excitation antennas in the film area where $E_z = 0$. The location of the antennas is chosen to obtain two nearly parallel spin wave beams. The simulation parameters remain the same as above, except for the size of the film (see Appendix for details). Figure 7(a) depicts an analysis of the isofrequency curves for the SW propagation across the \mathbf{E} -field boundary at $-11.4 \mu\text{m}^{-1} < k_y < 11.4 \mu\text{m}^{-1}$, $k_x < 0$, and $E_z > 0$. Figure 7(b) shows the micromagnetic simulation results for this process. It can be seen that in the part of the YIG film with $E_z > 0$, there is spin-wave focusing induced by DM-like interaction.

Suppose the \mathbf{E} field changes its sign to $E_z < 0$, then the isofrequency curve at $k_x < 0$ has only a positive Gauss curvature, Fig. 7(c). It causes the divergence of two parallel SW beams incident on the \mathbf{E} -field boundary. This is evidenced by the results of micromagnetic simulations propagation of two SW beams from the region with $E_z = 0$ to the region with $E_z < 0$ in Fig. 7(d). Here, the induced DM-like interaction leads to the divergence of the SWs. Therefore, the focusing or divergence of the SWs at the \mathbf{E} -field boundary can be changed by reversing the direction of the electric field normal to the film. For visual illustration, movies depicting the focusing and divergence of SW beams at the \mathbf{E} -field boundary can be found in the Supplemental Material [59] in the files 7b.mp4 and 7d.mp4.

Magnetization is perpendicular to the E-field boundary. Consider the situation when \mathbf{M}_S is normal to the \mathbf{E} -field boundary, Fig. 1(b). First, we analyze the propagation of the SW using isofrequency curves. Suppose the wave vector projection k_x of the incident dipolar-exchange SW is within the interval $-22.2 \mu\text{m}^{-1} < k_x < 22.2 \mu\text{m}^{-1}$, which covers all possible incidence angles. Like the conditions depicted in Fig. 5(a), in the geometry illustrated in Fig. 8(a), at $E_z = 0.35$ V/nm, the SW undergoes negative refraction when the wave numbers of the incident SW are in the range of $0 < k_x < 14.6 \mu\text{m}^{-1}$. The segment corresponding to this phenomenon is highlighted in orange on the isofrequency curve in Fig. 8(a). The positive refraction should be detected for the SWs with $-11.5 \mu\text{m}^{-1} < k_x < 0$ and $14.6 \mu\text{m}^{-1} < k_x < 22.2 \mu\text{m}^{-1}$. The incident wave must have wave numbers within the interval $-22.2 \mu\text{m}^{-1} < k_x < -11.5 \mu\text{m}^{-1}$ for the existence of the total internal reflection.

When the projection of the \mathbf{E} field changes its sign to the opposite ($E_z = -0.35$ V/nm), all limits of intervals k_x change their sign as well [Fig. 8(b)]. This happens because of a linear dependence of $\omega(E, k)$ concerning E, k_x according to Eqs. (7)–(10). The incident SWs with positive k_x values do not exhibit negative refraction, but it occurs at $-14.6 \mu\text{m}^{-1} < k_x < 0$. When $0 < k_x < 11.5 \mu\text{m}^{-1}$ and $-22.2 \mu\text{m}^{-1} < k_x < -14.6 \mu\text{m}^{-1}$, there is positive refraction. The total reflection takes place for $11.5 \mu\text{m}^{-1} < k_x < 22.2 \mu\text{m}^{-1}$.

All this analysis is confirmed by the results of micromagnetic simulations, depicted in Figs. 8(a) and 8(b), respectively. The directions of the simulated group velocities and wave vectors of the incident and refracted SWs coincide almost entirely with the corresponding vectors on the isofrequency curves. Therefore, when \mathbf{M}_S is normal to the \mathbf{E} -field boundary, the effects of SW refraction depend not only on the sign of

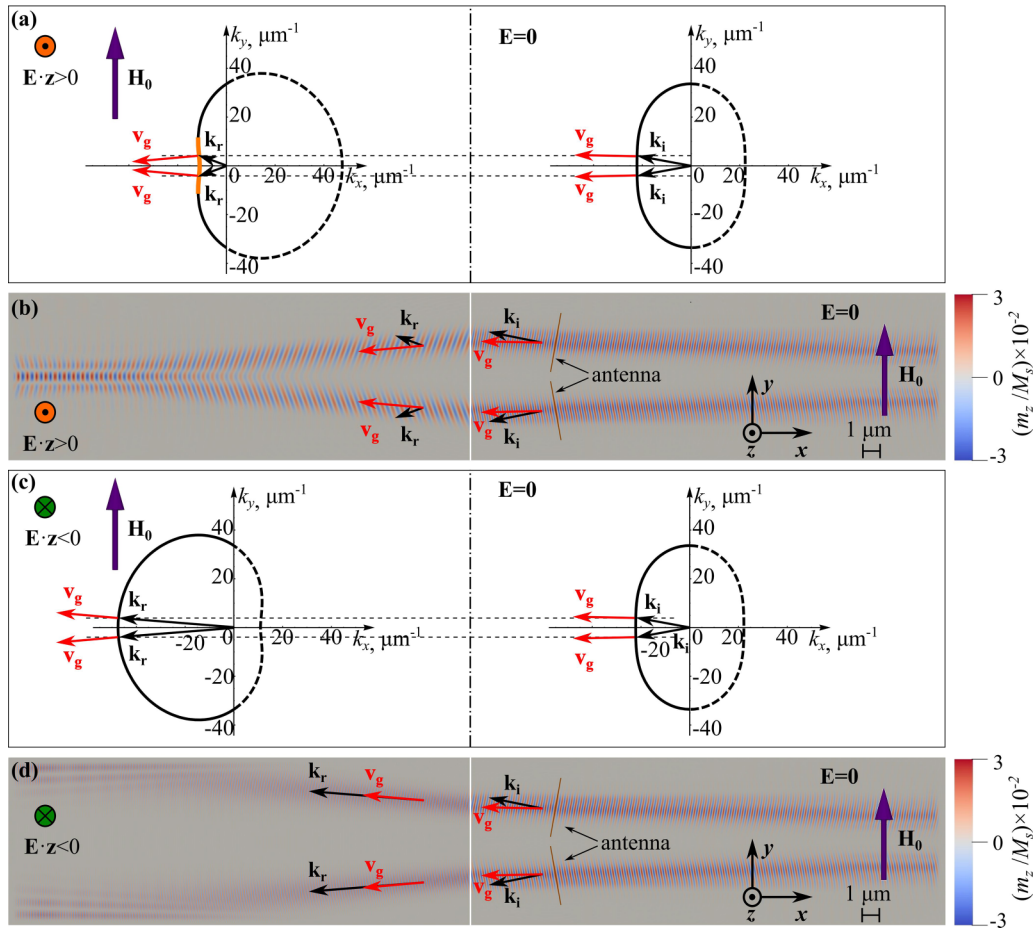


FIG. 7. Electric field control of focusing/divergence dipole-exchange SWs on the boundary of the magnetic film consisting of two half-spaces, with $|E_z| = 0.35$ V/nm and $E_z = 0$ for $\mathbf{H}_0 \parallel \mathbf{M}_S$. The SW frequency $f = 7.9$ GHz. The area with a negative refraction effect corresponds to the orange line. (a), (b) Analysis of the isofrequency curves and micromagnetic simulations for $E_z > 0$; (c) and (d) are the same as (a) and (b) but for $E_z < 0$.

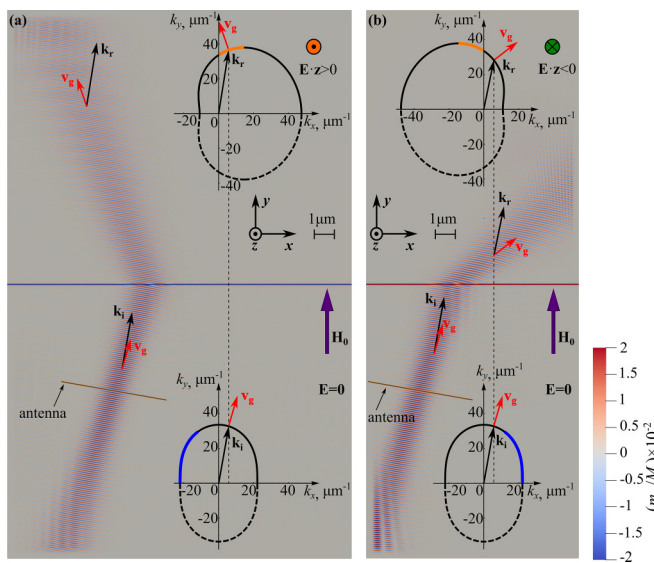


FIG. 8. Same as Fig. 6 but for $\mathbf{H}_0 \parallel \mathbf{M}_S$ normal to the boundary and a shift of the isofrequency curve along the boundary. The blue segment is the area of incident angles where SW is completely reflected.

the \mathbf{E} field but also on the sign of the incidence angle at the interface between electrically polarized and unpolarized parts of the magnetic film.

As already mentioned, even in a ferromagnet where the inversion symmetry is presented, an external electric field causes a phase shift of the SW that is linear both in the SW wave vector and in the applied electric field. This is an example of a topological effect (the AC phase) in magnetization dynamics [21–25]. Experimental data for YIG [20,27] confirmed that the electrical tuning of the SW phase in thin ferromagnetic films could be realized with high efficiency. Just this topological effect—the additional phase shift by the \mathbf{E} field—is seen in Figs. 6 and 8 for the refracted SW. The refraction processes depicted in Figs. 6(a), 6(b) 8(a), and 8(b) are illustrated in the Supplemental Material [59] by movies in the files 6a.mp4, 6b.mp4, 8a.mp4, 8b.mp4, respectively. The DM-like interaction strength induced by the electric field can be directly estimated by measuring the angle of the two refracted SW beams for positive and negative \mathbf{E} -field directions. Micromagnetic simulations demonstrate that this electric tuning can be highly efficient for the dipolar-exchange SW regime, and the DM-like interaction (the AC-phase effect) induced by an external electric field

can be used to control the SW power flow direction in a waveguide.

VI. CONCLUSIONS

Like in optics, where waveguides play a significant role in data processing, SW guides are key cells in magnonics. In recent years, immense experimental progress has been made in generating, detecting, and manipulating SW characteristics in nanoscale ferromagnetic films [14,15,20,61]. The obtained results provide a basic understanding of SWs' unique properties for data processing and information transmission in magnonic devices. Several methods have been proposed to use an artificially induced DM interaction that leads to a nontrivial asymmetric dispersion relation of SWs, enabling manipulation of the phase and propagation direction of SWs.

In this paper, we considered the possibility of tuning the strength of DM-like interaction in different regions of a homogeneous magnetic film by an external electric field. Through analytical calculations and micromagnetic simulations, we demonstrated that in a homogeneous magnetic material, there is the possibility of the static electric field control over the refraction of SWs at the interface formed by the regions under the effect of different electric fields. This is possible due to the electrically induced Aharonov-Casher phase shift of the SW phase (the DM-like interaction caused by the electric field). As in the case of SW propagation and refraction at the interface of magnetic films with different DM strengths [30–35], the systems under consideration are an ideal platform for versatile SW guides. We have shown that the external electric field control of SW refraction regimes in magnetic film, up to changing SW refraction from negative to positive and vice versa, can be helpful for the development and design of electrically controlled magnonic devices. From the fundamental point of view, the discussed peculiar phenomena open an avenue for quantifying topological effects in magnetization dynamics.

In conclusion, condensed matter physics is revolutionizing by introducing topology-grounded concepts that characterize the system's physical states and properties [62–64]. A representative case of topological effects on equilibrium magnetization dynamics has been discussed in this paper. The laser electric field can cause a dynamic phenomenon with topological effects on magnon dynamics, which local perturbations cannot disturb. Such theoretical proposals for controlling magnetization dynamics based on the Aharonov-Casher effect induced by laser electric field gradients have been discussed in Refs. [65,66]. The Aharonov-Casher effect generally provides a perspective direction for developing ultrafast topological magnonics. It is among all recent scientific discoveries linked to topological effects in condensed matter.

ACKNOWLEDGMENTS

The authors thank O. Gorobets and R. Verba for stimulating discussions and Stefan Blügel and M. Belogolovskii for reading the manuscript and providing valuable remarks. A.S.S. is grateful to the European Research Council for financial support under the European Union's Horizon 2020 research and innovation program (Grant No. 856538, project

“3D MAGiC”). V.N.K. acknowledges the financial support by the STCU, project “Magnetism in Ukraine Initiative,” Project Agreement No. 9918.

APPENDIX

Our micromagnetic simulation results were obtained by solving the time-dependent Landau-Lifshitz-Gilbert equation using the “MuMax3” code [54]. The material parameters we used for YIG are as follows: $\gamma = 1.761 \times 10^{11}$ rad/(s · T), $\mu_0 = 4\pi \times 10^{-7}$ H/m, $M_S = 140.5$ kA/m, $\mu_0 H_0 = 0.2$ T, $J = 2A/(\mu_0 M_S^2)$, where A stands for the exchange stiffness, $A = 3.7$ pJ/m [55], $\xi_{SO}^{-1} = 19$ eV [18–20], the Gilbert damping constant 10^{-4} [67]. These material parameters were also used to construct isofrequency curves based on Eqs. (7)–(10). According to [56], the anisotropy constant $K_u = 4300$ J/m³ was chosen for the film thickness $d = 10$ nm in the case of the simulation of exchange SWs, and $K_u = 4600$ J/m³ for $d = 30$ nm in the case of the simulation of dipole-exchange SWs. The choice of film thickness was determined by the quasi-uniform profile of the dynamic magnetization's normal component in the cases of exchange and dipole-exchange SWs. We used the film size of $6.5 \mu\text{m} \times 2.5 \mu\text{m} \times 10$ nm with the cell size $10 \text{ nm} \times 10 \text{ nm} \times 2.5 \text{ nm}$ for micromagnetic simulations of exchange SWs' refraction. The simulations of dipole-exchange SWs were done with two sizes of the film: (i) for the SWs' refraction, the film size was $26 \mu\text{m} \times 10 \mu\text{m} \times 30$ nm; (ii) $55 \mu\text{m} \times 10 \mu\text{m} \times 30$ nm for the focusing of dipole-exchange SWs. The films were discretized in the latter two cases with $10 \text{ nm} \times 10 \text{ nm} \times 10$ nm cubic-shaped elements. Thus, the cell sizes are smaller than the exchange length of YIG $l_{ex} = \sqrt{2A/(\mu_0 M_S^2)} \approx 17$ nm. We supposed that one-half of the film has a DM-like interaction induced by a perpendicular static electric field \mathbf{E} . In this case, the vector of the DM-like interaction is parallel to the film plane. The boundary between the two regions with $|\mathbf{E}| \neq 0$ and $|\mathbf{E}| = 0$ is a straight line. We simulated two cases corresponding (i) to the static magnetization vector $\mathbf{M}_S \parallel \mathbf{H}_0$ parallel to the boundary line and (ii) to $\mathbf{M}_S \parallel \mathbf{H}_0$ perpendicular to the boundary line. Such orientations of the \mathbf{E} and \mathbf{M}_S permit the realization of the Lifshitz invariants and boundary conditions [37], corresponding to interfacially induced DM-like interaction in Mumax3 [54,68]. The value of the DM-like interaction caused by the electric field is chosen according to [19,37].

The simulations consisted of two parts for all considered geometries. In the first part, the magnetization of the film was relaxed in the magnetic field \mathbf{H}_0 to an equilibrium configuration. Then, the perpendicular static electric field \mathbf{E} was applied to half of the film. Its values were $|\mathbf{E}| = 0.35$ V/nm for the simulation of the dipole-exchange SWs and $|\mathbf{E}| = 0.7$ V/nm for one of the exchange SWs.

In the second part of the simulations, the SW propagation was studied. We used the method described in Ref. [52] to generate the SW beam. The exciting magnetic field $\mathbf{h}_{ac}|_z$ is supposed to be located on the film side with $|\mathbf{E}| = 0$ under the rectangle area (denoted as the antenna in Figs. 4–8). For this area, the space-time dependence of the exciting magnetic field is described as $h_{ac}(x', y', t) = h(x', y') \sin(2\pi ft)$; here x', y' is a local coordinate system

with the x' axis parallel to the long side of the rectangle excited area (antenna) and the y' axis perpendicular to the expected wave front, $h(x', y') = h_0 \exp[-2(x' - x_0')^2 / (l \cdot \sigma)^2] \cdot f_H(y' - y_0' + w/2) \cdot f_H(-y' + y_0' + w/2)$, f_H is the Heaviside step function, l and w are length and width of the excitation area (see also [52]). In our simulations, we adopt the following parameters: $\sigma = 0.2$, $\mu_0 h_0 = 0.004$ T; $l = 5 \mu\text{m}$, $w = 30$ nm, time step $\Delta t = 0.1$ ps, $f = 7.9$ GHz for dipole-exchange SWs and $l = 1.5 \mu\text{m}$, $w = 10$ nm, $\Delta t = 0.025$ ps, $f = 50$ GHz in the case of the exchange SWs. The angle between the long side of the antenna and the

E-field boundary was $\pm 10^\circ$ for dipole-exchange SWs and $\pm 5^\circ$ for exchange SWs. The parabolic absorbing boundary conditions [69] were applied at the film edges $x = 0$, $x = L_x$ and $y = 0$, $y = L_y$, to decrease the intensity of the reflected SW. The width of the absorbing areas near the edges, where the damping parameter increases parabolically from 10^{-4} to 1, is equal to 3–5 SW wavelengths.

The estimated differences between corresponding values of the refracted wave vectors obtained from (7)–(10) (see Figs. 4–8) and from the micromagnetic simulations are less than 1.5%.

- [1] S. Neusser and D. Grundler, Magnonics: Spin waves on the nanoscale, *Adv. Mater.* **21**, 2927 (2009).
- [2] V. V. Kruglyak, S. O. Demokritov, and D. Grundler, Magnonics, *J. Phys. D: Appl. Phys.* **43**, 264001 (2010).
- [3] B. Lenk, H. Ulrichs, F. Garbs, and M. Münzenberg, The building blocks of magnonics, *Phys. Rep.* **507**, 107 (2011).
- [4] S. O. Demokritov and A. N. Slavin, *Magnonics – From Fundamentals to Applications* (Springer-Verlag, Berlin, 2013).
- [5] M. Weisheit, S. Fähler, A. Marty, Y. Souche, C. Poinsignon, and D. Givord, Electric field-induced modification of magnetism in thin-film ferromagnets, *Science* **315**, 349 (2007).
- [6] C.-G. Duan, J. P. Velev, R. F. Sabirianov, Z. Zhu, J. Chu, S. S. Jaswal, and E. Y. Tsymlal, Surface magnetoelectric effect in ferromagnetic metal films, *Phys. Rev. Lett.* **101**, 137201 (2008).
- [7] M. Tsujikawa and T. Oda, Finite electric field effects in the large perpendicular magnetic anisotropy surface Pt/Fe/Pt(001): A first-principles study, *Phys. Rev. Lett.* **102**, 247203 (2009).
- [8] R. Verba, V. Tiberkevich, I. Krivorotov, and A. Slavin, Parametric excitation of spin waves by voltage-controlled magnetic anisotropy, *Phys. Rev. Appl.* **1**, 044006 (2014).
- [9] D. A. Gilbert, A. J. Grutter, E. Arenholz, K. Liu, B. J. Kirby, J. A. Borchers, and B. B. Maranville, Structural and magnetic depth profiles of magneto-ionic heterostructures beyond the interface limit, *Nat. Commun.* **7**, 12264 (2016).
- [10] I. V. Zavislyak, M. A. Popov, and G. Srinivasan, Current-induced nonlinear magnetoelectric effects in strontium hexaferrite, *Phys. Rev. B* **94**, 224419 (2016).
- [11] T. Srivastava, M. Schott, R. Juge, V. Křížáková, M. Belmeguenai, Y. Roussigné, A. Bernard-Mantel, L. Ranno, S. Pizzini, S.-M. Chérif *et al.*, Large-voltage tuning of Dzyaloshinskii–Moriya interactions: A route toward dynamic control of skyrmion chirality, *Nano Lett.* **18**, 4871 (2018).
- [12] T. Koyama, Y. Nakatani, Ju. Ieda, and D. Chiba, Electric field control of magnetic domain wall motion via modulation of the Dzyaloshinskii–Moriya interaction, *Sci. Adv.* **4**, eaav0265 (2018).
- [13] F. Matsukura, Y. Tokura, and H. Ohno, Control of magnetism by electric fields, *Nat. Nanotechnol.* **10**, 209 (2015).
- [14] C. Song, B. Cui, F. Li, X. Zhou, and F. Pan, Recent progress in voltage control of magnetism: materials, mechanisms, and performance, *Prog. Mater. Sci.* **87**, 33 (2017).
- [15] B. Rana and Y. Otani, Towards magnonic devices based on voltage-controlled magnetic anisotropy, *Commun. Phys.* **2**, 90 (2019).
- [16] D. L. Mills and I. E. Dzyaloshinskii, Influence of electric fields on spin waves in simple ferromagnets: Role of the flexoelectric interaction, *Phys. Rev. B* **78**, 184422 (2008).
- [17] H. Katsura, N. Nagaosa, and A. V. Balatsky, Spin current and magnetoelectric effect in noncollinear magnets, *Phys. Rev. Lett.* **95**, 057205 (2005).
- [18] T. Liu and G. Vignale, Electric control of spin currents and spin-wave logic, *Phys. Rev. Lett.* **106**, 247203 (2011).
- [19] T. Liu and G. Vignale, Flexoelectric phase shifter for spin waves, *J. Appl. Phys.* **111**, 083907 (2012).
- [20] X. Zhang, T. Liu, M. E. Flatté, and H. X. Tang, Electric-field coupling to spin waves in a centrosymmetric ferrite, *Phys. Rev. Lett.* **113**, 037202 (2014).
- [21] Y. Aharonov and A. Casher, Topological quantum effects for neutral particles, *Phys. Rev. Lett.* **53**, 319 (1984).
- [22] Z. Cao, X. Yu, and R. Han, Quantum phase and persistent magnetic moment current and Aharonov–Casher effect in a $s = 1/2$ mesoscopic ferromagnetic ring, *Phys. Rev. B* **56**, 5077 (1997).
- [23] T. Fujita, M. B. A. Jalil, S. G. Tan, and S. Murakami, Gauge fields in spintronics, *J. Appl. Phys.* **110**, 121301 (2011).
- [24] X. S. Wang, H. W. Zhang, and X. R. Wang, Topological magnonics: A paradigm for spin-wave manipulation and device design, *Phys. Rev. Appl.* **9**, 024029 (2018).
- [25] V. N. Krivoruchko, Aharonov–Casher effect and electric field control of magnetization dynamics, *Low Temp. Phys.* **46**, 820 (2020).
- [26] V. Basso and P. Ansalone, Electric field effect on spin waves: Role of magnetic moment current, *Europhys. Lett.* **130**, 17008 (2020).
- [27] R. O. Serha, V. I. Vasyuchka, A. A. Serga and B. Hillebrands, Towards an experimental proof of the magnonic Aharonov–Casher effect, *Phys. Rev. B* **108**, L220404 (2023).
- [28] V. N. Krivoruchko, A. S. Savchenko, and V. V. Kruglyak, Electric-field control of spin-wave power flow and caustics in thin magnetic films, *Phys. Rev. B* **98**, 024427 (2018).
- [29] A. S. Savchenko and V. N. Krivoruchko, Electric-field control of nonreciprocity of spin wave excitation in ferromagnetic nanostripes, *J. Magn. Magn. Mater.* **474**, 9 (2019).
- [30] W. Yu, J. Lan, R. Wu, and J. Xiao, Magnetic Snell’s law and spin-wave fiber with Dzyaloshinskii–Moriya interaction, *Phys. Rev. B* **94**, 140410(R) (2016).
- [31] Zh. Wang, B. Zhang, Y. Cao, and P. Yan, Probing the Dzyaloshinskii–Moriya interaction via the propagation of spin

- waves in ferromagnetic thin films, *Phys. Rev. Appl.* **10**, 054018 (2018).
- [32] J. Mulkers, B. Van Waeyenberge, and M. V. Milošević, Tunable Snell's law for spin waves in heterochiral magnetic films, *Phys. Rev. B* **97**, 104422 (2018).
- [33] Z. Wang, Y. Cao, and P. Yan, Goos-Hänchen effect of spin waves at heterochiral interfaces, *Phys. Rev. B* **100**, 064421 (2019).
- [34] W. Bao, Zh. Wang, Y. Cao, and P. Yan, Off-axial focusing of a spin-wave lens in the presence of Dzyaloshinskii-Moriya interaction, *Phys. Rev. B* **102**, 014423 (2020).
- [35] F. Zhuo, Hang Li, Z. Cheng, and A. Manchon, Magnonic metamaterials for spin-wave control with inhomogeneous Dzyaloshinskii-Moriya interactions, *Nanomaterials* **12**, 1159 (2022).
- [36] X. Wang, L. Chotorlishvili, G. Guo, and J. Berakdar, Electric control of emergent magnonic spin current and dynamic multiferroicity in magnetic insulators at finite temperatures, *Phys. Lett. A* **382**, 1100 (2018).
- [37] X. Wang, L. Chotorlishvili, G. Guo, and J. Berakdar, Electric field controlled spin waveguide phase shifter in YIG, *J. Appl. Phys.* **124**, 073903 (2018).
- [38] V. N. Krivoruchko, A. S. Savchenko, Electric field control of spin-wave refraction in thin ferromagnetic film, in *Proceedings of the 2019 IEEE 9th International Conference Nanomaterials: Applications Properties* (IEEE, Odesa, Ukraine, 2019).
- [39] J. Fernandez-Rossier, M. Braun, A. S. Nunez, and A. H. MacDonald, Influence of a uniform current on collective magnetization dynamics in a ferromagnetic metal, *Phys. Rev. B* **69**, 174412 (2004).
- [40] P. Lederer and D. L. Mills, Possible experimental test of the band theory of magnetism, *Phys. Rev.* **148**, 542 (1966).
- [41] V. Vlaminck and M. Bailleul, Current-induced spin-wave Doppler shift, *Science* **322**, 410 (2008).
- [42] B. A. Kalinikos and A. N. Slavin, Theory of dipole-exchange spin wave spectrum for ferromagnetic films with mixed exchange boundary conditions, *J. Phys. C: Solid State Phys.* **19**, 7013 (1986).
- [43] S.-K. Kim, S. Choi, K.-S. Lee, D.-S. Han, D.-E. Jung, and Y.-S. Choi, Negative refraction of dipole-exchange spin waves through a magnetic twin interface in restricted geometry, *Appl. Phys. Lett.* **92**, 212501 (2008).
- [44] F. Ma and Y. Zhou, Interfacial Dzyaloshinskii-Moriya interaction induced nonreciprocity of spin waves in magnonic waveguides, *RSC Adv.* **4**, 46454 (2014).
- [45] R. A. Gallardo, D. Cortés-Ortuño, T. Schneider, A. Roldán-Molina, Fusheng Ma, R. E. Troncoso, K. Lenz, H. Fangohr, J. Lindner, and P. Landeros, Flat bands, indirect gaps, and unconventional spin-wave behavior induced by a periodic Dzyaloshinskii-Moriya interaction, *Phys. Rev. Lett.* **122**, 067204 (2019).
- [46] J. Chen, H. Yu, and G. Gubbiotti, Unidirectional spin-wave propagation and devices, *J. Phys. D: Appl. Phys.* **55**, 123001 (2022).
- [47] J. Stigloher, M. Decker, H. S. Korner, K. Tanabe, T. Moriyama, T. Taniguchi, H. Hata, M. Madami, G. Gubbiotti, K. Kobayashi, T. Ono, and C. H. Back, Snell's law for spin waves, *Phys. Rev. Lett.* **117**, 037204 (2016).
- [48] J.-V. Kim and R. L. Stamps, and R. E. Camley, Spin wave power flow and caustics in ultrathin ferromagnets with the Dzyaloshinskii-Moriya interaction, *Phys. Rev. Lett.* **117**, 197204 (2016).
- [49] W. Zhen and D. Deng, Giant Goos-Hänchen shift of a reflected spin wave from the ultrathin interface separating two antiferromagnetically coupled ferromagnets, *Optics Communic.* **474**, 126067 (2020).
- [50] Y. S. Dadoenkova, N. N. Dadoenkova, I. L. Lyubchanskii, M. L. Sokolovskyy, J. W. Klos, J. Romero-Vivas, and M. Krawczyk, Huge Goos-Hänchen effect for spin waves: A promising tool for study magnetic properties at interfaces, *Appl. Phys. Lett.* **101**, 042404 (2012).
- [51] P. Gruszecki, J. Romero-Vivas, Y. S. Dadoenkova, N. N. Dadoenkova, I. L. Lyubchanskii, and M. Krawczyk, Goos-Hänchen effect and bending of spin wave beams in thin magnetic films, *Appl. Phys. Lett.* **105**, 242406 (2014).
- [52] P. Gruszecki, Y. S. Dadoenkova, N. N. Dadoenkova, I. L. Lyubchanskii, J. Romero-Vivas, K. Y. Guslienko, and M. Krawczyk, Influence of magnetic surface anisotropy on spin wave reflection from the edge of ferromagnetic film, *Phys. Rev. B* **92**, 054427 (2015).
- [53] P. Gruszecki, M. Mailyan, O. Gorobets, and M. Krawczyk, Goos-Hänchen shift of a spin-wave beam transmitted through anisotropic interface between two ferromagnets, *Phys. Rev. B* **95**, 014421 (2017).
- [54] A. Vansteenkiste, J. Leliaert, M. Dvornik, M. Helsen, F. Garcia-Sanchez, and B. Van Waeyenberge, The design and verification of MuMax3, *AIP Adv.* **4**, 107133 (2014).
- [55] S. Klingler, A. V. Chumak, T. Mewes, B. Khodadadi, C. Mewes, C. Dubs, O. Surzhenko, B. Hillebrands, and A. Conca, Measurements of the exchange stiffness of YIG films using broadband ferromagnetic resonance techniques, *J. Phys. D: Appl. Phys.* **48**, 015001 (2015).
- [56] A. Talalaevskij, M. Decker, J. Stigloher, A. Mitra, H. S. Körner, O. Cespedes, C. H. Back, and B. J. Hickey, Magnetic properties of spin waves in thin yttrium iron garnet films, *Phys. Rev. B* **95**, 064409 (2017).
- [57] J. Mulkers, B. Van Waeyenberge, and M. V. Milošević, Effects of spatially engineered Dzyaloshinskii-Moriya interaction in ferromagnetic films, *Phys. Rev. B* **95**, 144401 (2017).
- [58] A. Raeliarijaona, R. Nepal, and A. A. Kovalev, Boundary twists, instabilities, and creation of skyrmions and antiskyrmions, *Phys. Rev. Mater.* **2**, 124401 (2018).
- [59] See Supplemental Material at <http://link.aps.org/supplemental/10.1103/PhysRevB.109.184437> for movies of spin-wave refraction corresponding to the Figs. 4–8, obtained from micromagnetic simulations.
- [60] R. A. Gallardo, P. Alvarado-Seguel, A. Kákay, J. Lindner, and P. Landeros, Spin-wave focusing induced by dipole-dipole interaction in synthetic antiferromagnets, *Phys. Rev. B* **104**, 174417 (2021).
- [61] Y. Shiota, R. Hisatomi, T. Moriyama, and T. Ono, Observation of the dispersion relations for quantized coherent spin waves excited by a microwave antenna, *Phys. Rev. B* **102**, 214440 (2020).
- [62] S. Blügel, Y. Mokrousov, T. Schapers, and Y. Ando (eds.), *Topological Matter – Topological Insulators, Skyrmions and Majoranas*. 48th IFF Spring School (Forschungszentrum Jülich/Key Technologies, Jülich, 2017).

- [63] R. Streubel, P. Fischer, F. Kronast, V. P. Kravchuk, D. D. Sheka, Y. Gaididei, O. G. Schmidt, and D. Makarov, Magnetism in curved geometries, *J. Phys. D: Appl. Phys.* **49**, 363001 (2016).
- [64] Y. Tokura and K. Yasuda, and A. Tsukazaki, Magnetic topological insulators, *Nat. Rev. Phys.* **1**, 126 (2019).
- [65] K. Nakata, S. K. Kim, and J. Klinovaja, and D. Loss, Magnonic topological insulators in antiferromagnets, *Phys. Rev. B* **96**, 224414 (2017).
- [66] K. Nakata and S. K. Kim, and S. Takayoshi, Laser control of magnonic topological phases in antiferromagnets, *Phys. Rev. B* **100**, 014421 (2019).
- [67] C. Dubs, O. Surzhenko, R. Thomas, J. Osten, T. Schneider, K. Lenz, J. Grenzer, R. Hübner, and E. Wendler, Low damping and microstructural perfection of sub-40nm-thin yttrium iron garnet films grown by liquid phase epitaxy, *Phys. Rev. Mater.* **4**, 024416 (2020).
- [68] J. Leliaert, M. Dvornik, J. Mulkers, J. De Clercq, M. V. Milošević, and B. Van Waeyenberge, Fast micromagnetic simulations on GPU—Recent advances made with MuMax3, *J. Phys. D* **51**, 123002 (2018).
- [69] G. Venkat, H. Fangohr, and A. Prabhakar, Absorbing boundary layers for spin wave micromagnetics, *J. Magn. Magn. Mater.* **450**, 34 (2018).